Journal Pre-proof

Multifunctional porous SiC nanowire scaffolds

Yu Chen, Oluwafunmilola Ola, Guangsheng Liu, Lei Han, Mian Zahid Hussain, Kunyapat Thummavichai, Jiahao Wen, Linyi Zhang, Nannan Wang, Yongde Xia, Yanqiu Zhu

PII: S0955-2219(21)00104-7

DOI: https://doi.org/10.1016/j.jeurceramsoc.2021.02.021

Reference: JECS 13892

To appear in: *Journal of the European Ceramic Society*

Received Date: 15 January 2021

Revised Date: 10 February 2021

Accepted Date: 11 February 2021

Please cite this article as: Chen Y, Ola O, Liu G, Han L, Hussain MZ, Thummavichai K, Wen J, Zhang L, Wang N, Xia Y, Zhu Y, Multifunctional porous SiC nanowire scaffolds, *Journal of the European Ceramic Society* (2021), doi: https://doi.org/10.1016/j.jeurceramsoc.2021.02.021

Multifunctional porous SiC nanowire scaffolds

Yu Chen[a,b], Oluwafunmilola Ola[b+], Guangsheng Liu[a], Lei Han[b], Mian Zahid Hussain[b], Kunyapat Thummavichai[b], Jiahao Wen[a], Linyi Zhang[a], Nannan Wang[a,*], Yongde Xia[b], Yanqiu Zhu[a,b,*]

[a] *GIFT (Guangxi Institute for Fullerene Technology), Key Laboratory of New Processing Technology for Nonferrous Metals and Materials, Ministry of Education, School of Resources, Environment and Materials, Guangxi University, Guangxi 530004, China*

[b] *College of Engineering, Mathematics and Physical Sciences, University of Exeter, Exeter EX4 4SB, UK*

[+] New Address*: Advanced Materials Group, Faculty of Engineering, The University of Nottingham, Nottingham, NG7 2RD, United Kingdom*

Corresponding author:

*E-mail: wangnannan@gxu.edu.cn; Y.Zhu@exeter.ac.uk

Abstract

Porous SiC nanowire (SiCNW) ceramics have great potentials for engineering applications. We herein report the fabrication of 3D SiCNW scaffolds with tuneable microstructures, densities, and therefore properties, by regulating the solid loading content in the reticulated melamine foam (MF) template and finalizing with a modified carbothermal reaction. We first demonstrate the resulting samples exhibiting high strength (modulus up to ~167.3 kPa), good recoverability (11% residual strain and 72% maximum stress after 100 compressive cycles at a ε = 20%), low thermal conductivity of 32-54 mW $m^{-1}K^{-1}$ at room temperature, and good fire retardance performance. We further show that these unique and tuneable SiCNW scaffolds could act as efficient organic solvent/oil absorbent, as excellent support for MOF-derived TiO_2-C catalyst to achieve enhanced

photocatalytic performance, and as competent electromechanical strain sensors. These multifunctionalities could find niche applications in energy and environment devices.

Keywords: Melamine foam, SiC nanowire, Absorbent, Catalyst support, Strain sensor

1. Introduction

Porous SiC structures with open porosity, low density, low thermal conductivity, and excellent chemical inertness are appealing for applications including thermal insulators, filters, catalyst supports and absorbents. One of the most adopted approaches for the fabrication of porous SiC is the replica template technique, by impregnating a porous template in a pre-ceramic slurry, followed with drying and pyrolysis procedures. The template will be extracted during the high temperature pyrolysis, either via burning out or by decomposition, leaving behind a three-dimensional and open-celled structure mimicking the original template. Owing to the high permeability, light-weight, super-elasticity, and low-cost, polymeric sponges such as polyurethane (PU) foam or melamine foam (MF) are commonly selected as the template [1].

Generally, SiC porous ceramics produced by the replica template exhibit reticulated structures with hollow struts, after removing the original template [2]. However, secondary pores can be introduced as a result of gas evolution during the slurries decomposition or incomplete densification during sintering. Meanwhile, the stress concentration at the strut ends and around macropores raised from incomplete coverage of the template will give rise to the strength loss [3]. These defects could lead to brittle failure, therefore restricting the long-term service of the foam. To remove the structural imperfections, recoating or infiltrating porous ceramic with additional slurry has been attempted, but neither of them could effectively reduce the brittleness of the material. In this paper, incorporating SiC nanowires (SiCNWs) or directly creating SiCNW structures are considered as a promising alternative, since nanowires exhibit good flexibility with high modulus. In addition, the interconnected three-dimensional (3D) structure of SiCNWs with high specific surface area is attractive for applications in filtration or catalyst support [4].

Numerous studies have reported the template growth of SiCNWs via the polymer pyrolysis chemical vapor deposition (PPCVD) process. Li et al. fabricated a melamine foam-templated SiC nanowire aerogel using the PPCVD process [5]. In their work, they first carbonised the melamine foam, then soaked it into a catalyst solution, followed with the sintering process. The off-gas from

the pyrolysis of polycarbonsilane (PCS) was used as the SiCNW precursor, and by burning off the carbon foam they obtained the SiCNW aerogel. The biggest drawback of this approach is that the SiC source gases were introduced from outside of the template, which limited their reach to inside. Hence, it is difficult to create homogeneous distributions for the SiCNWs. This could cause degradation to the structural integrity and mechanical stability of the final products.

In this paper, we report the fabrication of 3D SiCNW scaffold by direct infiltrating the MF with SiO_2-sugar slurries, followed by a one-step, catalyst-free, in-situ carbothermal reaction between gaseous SiO_2 and sugar-derived active carbon. In this way, the MF with 3D connected framework not only served as a platform to regulate the growth of SiCNWs, but also participated in the carbothermal reaction for the creation of the SiC struts. The microstructural evolution, mechanical properties, and thermal conductivity of the resulting SiCNW scaffolds with tuneable densities have been investigated. Benefitting from the low density, special dual-structure, and good thermal and mechanical stability, the resulting SiCNW scaffolds also showed good performances as organic solvent/ oil absorbent, catalyst supports, and electromechanical sensors.

2. Experimental Methods

2.1 Materials

The slurries used for impregnating melamine foams (LTWHOME ltd. China) were prepared as following: The SiO_2 sol was made by hydrolysis of Tetraethyl orthosilicate (TEOS, 98%, Acros Organics), where TEOS, ethanol (≥ 99.8%, Sigma-Aldrich), and H_2O were mixed at a volume ratio of 2:2:1, HCl (37%, Sigma-Aldrich) as the pH modifier was then added to adjust the pH value of the solution to ~ 3. The sol was then subjected to magnetic stirring for 24 h. Subsequently, granular sugar (Whitworths Co.) was added to form the SiO_2-sugar slurries.

2.2 Synthesis of SiC nanowire scaffold

The preparation scheme for the SiCNW scaffolds is illustrated in Fig. 1. The commercial MF 35 × 35 × 35 mm^3 cubic blocks, as the template, were immersed in 50 ml pre-mixed SiO_2-sugar slurries, followed by a vacuum degassing process for 120 min to allow the slurries thoroughly filling the pores. After the immersion, compressive pressures were applied to the template, to remove the excessive slurry. The compressive strain is defined as:

$$\text{Compressive strain} = \frac{h_0 - h_1}{h_0} \times 100\%,$$

where h_0 is the original height of the template, and h_1 represents the height under compression.

The samples were then dried on a rotary machine at room temperature for 24 h, and in an oven at 100 °C for another 24 h, respectively. Upon sintering, the samples were first heated at 1 °C min^{-1} to 700 °C in order to preserve the original shape of MF, the calcination temperature was then increased to 1500 at 5°C/min, and kept for 3 h, under Ar atmosphere. Finally, purified SiC was obtained by burning off the superfluous carbon using a heat treatment at 800 °C in air for 2 h.

2.3 Surface modification of SiCNW scaffolds

SiCNW scaffolds were firstly ultrasonically washed in deionized water and ethanol for 20 min, respectively. After cleaning, they were dried in the oven at 80 °C for 24 h. The dried samples were immersed in a 1.0 vol% n-heptane solution of n-Octadecyltrichlorosilane (OTS) for 1 h at room temperature, after this, the samples were rinsed with ethanol and dried at 100 °C in the vacuum for 6 h.

2.4 Preparation of TiO_2-C/SiC composites

The NH_2-MIL-125(Ti) (Ti-MOF) containing organic linker and metal cluster with a molar ratio of 3:1 was prepared by dissolving 15 mM 2-aminoterephthalic acid and 5 mM $Ti(OBu)_4$ in 30 mL dimethylformamide (DMF) and 30 mL methanol. The as-obtained SiCNW scaffold was immersed in the mixed solution, which was subjected to a solvothermal reaction at 140 °C for 48 h. The final Ti-MOF/SiC composite was first washed twice with DMF to remove the unreacted species, followed by washing twice with methanol, and then dried overnight in an oven at 70 °C. To examine the benefit of the in-situ synthesized Ti-MOF on the SiCNW scaffold, an ex-situ catalyst loading was also carried out, as a reference, where the SiCNW scaffold was dip-coated by the as-synthesised Ti-MOF solutions for 48 h, followed with the same drying procedure.

The carbonisation of Ti-MOF/SiC was carried out by heating the sample to 800 °C for 1 h at a rate of 10 °C min^{-1} under Ar, and the TiO_2-C/SiC(*in-situ*) and TiO_2-C/SiC(*ex-situ*) composites were then obtained, respectively.

2.5 Characterisation and measurement

The bulk density of the samples was calculated from the weight-to-volume ratio, and the porosities were estimated from the ratio of the bulk density to the true density. XRD powder diffraction patterns were recorded on a Bruker D8 Advance diffractometer with a Cu Kα radiation (λ = 0.154 nm, operated at 40 kV and 40 mA), at a time interval of 1 s and a step size of 0.02°, within the 2θ range from 10° to 80°. SEM observations were performed using a Hitachi S3200N SEM-EDS

machine. Thermal gravimetric analysis was conducted using a TA SDT Q600 TGA-DSC instrument, at a ramping rate of 10 °C min^{-1} under air environment.

Thermal diffusivity evaluations of the materials were conducted on a NETZSCH LFA 467 HyperFlash machine. Prior to testing, the 1 cm^2 samples were spray-coated with a thin layer of graphite, to improve the signal to noise ratio and enhance the light emission/absorbance during analyses. The thermal conductivity (λ) was extrapolated from the dataset obtained from thermal diffusivities (α), using $\lambda = \alpha\rho Cp$, where ρ and Cp represent the density and specific heat capacity of the sample, respectively. An average value was obtained from the software after 3 runs.

The static compression test was carried out on a Lloyds EZ20 advanced universal mechanical testing system, using a 1 kN detection cell at a loading rate of 5 mm min^{-1}. The cyclic compression test for the SiCNW scaffolds at a pre-set strain of 20% was carried out on the same machine, but using a 50 N detection cell, at a loading rate of 8 mm min^{-1}.

Water wettability of samples was evaluated by measuring the water contact angle (WCA) using a video-based optical contact angle measuring system with a high-speed USB camera (DataPhysics OCA15Pro).

The photodegradation of organic dye methylene blue (MB) by the TiO_2-C/SiC composites was evaluated under UV-visible light irradiation. The UV-visible light source was provided by a 400 W Xe/Hg lamp. Typically, 250 mg of black TiO_2-C/SiC sample was added into 100 mL (10 ppm) aqueous MB solution. After different time intervals, 1 mL aliquots were taken out, and the concentration of MB was determined by a UV–vis absorption spectroscopy. The subsequent photodegradation (D) of MB in aqueous solution was calculated in terms of the decrease in final (C) and initial (Co) concentrations.

The pressure-dependent electrical response was analyzed using a KEITHLEY 2612B System, with the Sourcemeter Instruments that connected to a computer. The sample was placed between two parallel Au-plated Cu plate electrodes.

3 Results and Discussion

3.1 Fabrication of MF-templated 3D SiCNW structures

As illustrated in Fig. 1, the fabrication process started from immersing the melamine foam into a SiO_2-sugar slurry, then a fixed compression strain of ε = 80% was applied to remove the excessive slurry absorbed. Following the drying and sintering processes, the unreacted carbon was burnt off in

air, leaving behind the pure SiCNW scaffold. As the MF can hardly generate active gaseous C during the calcination, additional carbon source was therefore added for the creation of SiCNWs through carbothermal reduction of SiO_2. Owing to its abundant supply and low cost, kitchen-sugar was used in this study. The sugar also increased the viscosity of the slurries, which facilitated the attachment of slurry onto the MF networks. To optimise the slurry composition, slurries containing 5, 10, 15, and 20 wt.% of sugar were prepared, respectively, resulting in samples named as SiC-5%, SiC-10%, SiC-15%, and SiC-20%. The preparation conditions and the properties of resultant SiC scaffolds are summarised in Table S1. The solid loading and the volume of the resultant scaffolds increased linearly with the upgrade of sugar concentration, which is translated as that the higher viscosity of the slurries, the higher the solid loading. The increased solid loading better prevented the MF from shrinkage during the sintering stage.

Thermal gravimetric analysis (TGA) of all the as-obtained SiC/C samples was conducted between 20 and 1000 °C in air to investigate the content of remaining carbon and the temperature required for later carbon removal. As shown in Fig. 2(a), during heating the samples experienced a weight loss from 600 °C, corresponding to loss of unreacted C in the sample that was oxidised by air. The weight loss of sample SiC/C-5% was 20.2%, while it linearly increased to 35.9% for sample SiC/C-20%, as a result of the higher sugar concentration. Subsequently, in the temperature range of 700-1000 °C, all samples exhibited a slight weight gain due to the oxidation of SiC, after the carbon content was fully burnt off (oxidised). X-ray diffraction patterns (XRD) of the as-obtained samples are presented in Fig. 2(b). Three sharp peaks appear at 35.7°, 60°, 71.8° corresponding to the (111), (220), and (311) planes of the β-SiC phase, while the low intensity peak at around 33.5° represents the formation of stacking fault (S.F.) [6]. However, the result for sample SiC-5% is noticeably different from others, where the peak of SiO_2 that appears at 23° is dominant, indicating that the SiO_2 was not completely consumed despite the carbon was superfluous. Based on these results, a sugar concentration of at least 10% is prerequisite for consuming up all Si content. Meanwhile, an additional thermal treatment at 800 °C in air for 1 h was designed to remove the excessive carbon residue in the scaffold.

To illustrate the morphological evolution of SiCNW scaffolds, 3 sets of impregnated MF and their corresponding resultant SiC scaffolds: samples SiC-10%, SiC-15%, and SiC-20% were characterised by using scanning electron microscopy (SEM), as shown in Fig. S1. The MF framework was uniformly impregnated by slurries containing 10 wt.% of sugar and the interconnectivity of its struts was well-preserved. This crack-free microstructure feature indicates the good quality of the coating, since the drying process of the coated slurries frequently causes cracks due to shrinkage. The scaffold from the SiC-10% sample exhibited an open cell structure,

which dominantly constituted nanowires; meanwhile struts with morphology duplicating the original MF networks were visible. With the increase of sugar concentration to 15 wt.%, closed cells were identified in the coated MF samples, leading to the formation of a few SiC membranes. When the sugar concentration reached 20 wt.%, the open cellular structure within the MF was largely replaced by slurry membranes, and the growth of SiCNWs was significantly restricted due to the limited interconnectivity within the structure. A large number of SiC particles, instead of SiCNWs, was found in the SiC-20% sample. The microstructural features of these samples agreed with their variation of densities. The bulk densities of the SiC-15% and SiC-20% samples were considerably lower, due to their larger volumes, than that of the SiC-10% sample. These experimental results confirmed that slurries containing 10 wt.% sugar was optimal for the preparation of SiCNW scaffolds with homogeneous nanowire distribution. Furthermore, the EDS results indicated that both nanowires and struts from the SiC-10% sample were mainly composed of Si and C, with a trace amount of O, due to the inevitable oxidation of SiC (Fig. S2). It is obvious that the MF not only served as the matrix template for the growth of SiCNWs, but also participated in the reaction, giving rise to the SiC struts.

Upon heating, the SiO_2 sol decomposed and generated activated Si at around 160 ºC [7],[8]:

$$Si(OC_2H_5)_4\,(g) \rightarrow SiO_2\,(s) + 2H_2O + 4C_2H_4\,(g) \quad (1)$$

The sugar experienced a series of polymerisation, dehydrogenation, carbonisation, and graphitisation process during the thermal treatment [9]. Two types of carbothermal reaction between active C and SiO_2 occurred. One was the vapor-solid (VS) mechanism between gaseous SiO and CO, which gave rise to continuous growth of SiCNWs, according to the reaction (2):

$$SiO\,(g) + 3CO\,(g) \rightarrow SiC\,(s) + 2CO\,(g) \quad (2)$$

while the other was solid/liquid-solid reaction between SiO_2 and the carbonised MF, which created the SiC struts:

$$SiO_2\,(s,l) + 2C\,(s) \rightarrow SiC\,(s) + CO_2\,(g) \quad (3)$$

In the replica template method, the solid loading of preceramic slurries played a critical role in determining the final microstructure and properties of the resultant materials. The most common strategy to manipulate the solid loading is by adjusting the concentration of slurries. In this study, we developed a more efficient way to change the solid loading, by simply varying the compressive

strains (90%, 70%, 50%, respectively) applied to remove the excessive slurries from the MF (Fig. 3(a)). As outlined in Fig. 3(b), both the slurry loading content on the MF and the density of the resulting samples kept a good linear relationship with the compressive strains applied. The density of the scaffolds increased from 57.8 to 165.6 mg cm^{-3}, as a result of rising solid loading. The three samples according to their densities are denoted as SiC-light (SiC-l), SiC-medium (SiC-m), and SiC-heavy (SiC-h), respectively.

In the SiC-l sample (Fig. 3(c)), the framework morphology of the original MF was preserved very well, and the framework consisted of interweaving SiCNWs. With higher solid loading in the SiC-m sample, broken and shrunken struts were less distinguishable due to the improved surface tension from the coated slurries, as shown in Fig. 3(d). However, the increased intensity of carbothermal reaction created visibly denser SiCNWs, which might be accountable for the increased density, as compared with SiC-l. For sample SiC-h with the highest density, the SiC membranes appeared, and the growth of the SiCNWs was therefore partially restricted. (Fig. 3(e)). The microstructure of ultralong SiCNWs was further characterised, they exhibited diameters ranging from 20-110 nm (Fig. 3(f)), with majority in the range of 40-70 nm (inset of Fig. 3(f)). The transmission electron microscopy (TEM) images and the corresponding selected area electron diffraction (SAED) results revealed that the SiCNWs were single crystallised, and grew along the [111] direction, with visible stacking faults (Fig. 3(g) and (h)). This atomic information is in agreement with the sharp diffraction peaks and S.F. peak in the XRD patterns. The morphological evolution of SiCNW scaffolds and its dependence on the solid loading are summarised in Fig. 3(i).

3.2 Properties of the SiCNW scaffolds

The MF-templated growth could lead to lightweight scaffolds with intended shapes consisting of uniformly distributed SiCNWs, as shown in Fig. 4(a) and (b). Fig. 4(c) displays the uniaxial compressive responses of as-obtained SiC scaffolds at a strain setting of $\varepsilon = 70\%$. The σ-ε curves exhibited a typical three-stage deformation regime for porous ceramic structures. The SiC-l and SiC-m samples showed a linear elastic regime for $\varepsilon < \sim 35\%$ and $\varepsilon < \sim 30\%$, respectively, followed with a plateau stage and densification regime for $\varepsilon > \sim 55\%$ with σ increasing sharply, as a result of the stacking of SiC struts and nanowires. However, the elastic regime of the SiC-h sample was merely $\varepsilon < \sim 10\%$, followed with small drops at $\varepsilon = 50\%$ and 63%, raising from the breakage of SiC membranes. As shown in the enlarged σ-ε curves of the elastic region (Fig. 4(d)), unlike other nanowire structures that exhibit smooth curves, all present scaffolds demonstrated a dynamic strain aging phenomenon, with an apparent serrated yielding in the curves. This phenomenon can be

ascribed to the deformation and failure of SiC struts and cells, specifically for the SiC-h sample. However, the brittle failure manner for ceramics was completely absent. By fitting the σ-ε curve in the linear elastic region, a Young's Modulus of ~32.1, 76.5, and 167.3 kPa was obtained for the SiC-l, SiC-m, and SiC-h scaffold, respectively. Furthermore, their relative compressive modulus (E/E_s) as a function of relative density (ρ/ρ_s) was plotted and compared with other typical nanostructures reported (Fig. 4(e)). A quantitative scaling behavior of $(E/E_s) \sim (\rho/\rho_s)^n$ was obtained, with $n \approx 1.64$ as the scaling exponent. This value suggests an efficient stress dissipation through the uniform structure, demonstrating a good self-supporting stability. Al_2O_3 microlattices with a scaling exponent of merely $n \approx 1.1$ exhibited a stretch-dominated deformation [10], whilst most low-density nanostructures such as freeze-cast SiC networks [11], Si_3N_4 nanobelt aerogels [12], and CNT foam [13], exhibited a steeper scaling factor ($2 \leq n \leq 3$), owing to the bending-dominated deformation mechanism. The present SiCNW scaffolds with a scaling exponent within the range of 1-2 were originated from the co-existence of nanowire constituent and the cellular structures, as revealed by the SEM study.

To examine the recoverability of SiC scaffolds, loading-unloading compression cycles at a strain of $\varepsilon = 20\%$ were performed and the results were displayed in Fig. 4(f-h). During the consecutive compression, all the SiCNW scaffolds experienced the decrease of maximum stress and strain retention in the first 10 cycles but remained constant in the following cycles. The SiC-l preserved a 72% of the max stress, and 89% strain retention after 100 loading-unloading cycles, demonstrating a good cyclic fatigue resistance, better off the other two samples. The better resilience was attributed to the well-preserved SiC struts, which played a critical role in maintaining the structural integrity of the SiCNW scaffolds. Furthermore, the significant hysteresis is observed in the σ-ε curves, indicating effective energy dissipation. For SiC-l sample, the work done in the loading process of the first cycle is calculated to be ~60 mJ cm^{-3}, and the energy dissipation to be ~24 mJ cm^{-3}, yielding an energy loss coefficient of ~0.60. After 100 cycles, the coefficient remains constant at ~0.15 (Fig. S4), suggesting the possibility for energy damping materials. The SiC-m also demonstrates the good capability of energy dissipation, with an energy loss coefficient of ~0.13 after 100 cycles. Whilst this value for SiC-h is merely ~0.04 due to the poor recoverability.

Owing to the complex configuration with the co-existence of nanowire and struts, a thermal conductivity of merely ~32-54 mW $m^{-1}k^{-1}$ at room temperature was obtained. A comparison of the thermal conductivity between the as-obtained SiC scaffolds produced in this work and other reported porous ceramic (SiC and SiO_2) nanowire structures was shown in Fig. 4(i). The thermal conductivity of present SiCNW scaffolds is lower than other porous SiC foams with similar density, and even comparable to some SiC thermal insulation mats with much lower density, demonstrating

the outstanding thermal insulation capability of present scaffolds. As a demonstration of the thermal insulation performance, a SiCNW scaffold was placed on an alcohol lamp, a fresh flower was then loaded on top of the sample (Fig. S5). The flower exhibited little withering or carbonisation under the heating of an alcohol lamp for 10 min, highlighting the robust thermal insulation of the SiCNW scaffolds.

The thermal stability of SiCNW scaffold was investigated using thermalgravimetric analysis (TGA, Fig. 4(j)). The purified SiCNW scaffold demonstrated a great thermal stability as they experienced no weight loss during tests up to 700 °C. Additionally, the SiCNW scaffold exhibit fire-retardance, as shown in inset Fig. 4(j), no ignition or structural collapse was observed when the scaffolds were exposed to the high-temperature (~1300 °C) flame, they even exhibit elastic resilience after compressed at an ε of 20% upon burning, suggesting simultaneous excellent fire-resistance and temperature-invariant recoverability.

As shown in the spider chart (Fig. 4(k)), the advantages of these MF-templated SiCNW scaffolds are highlighted. Sample SiC-h with the highest mechanical strength could be a promising candidate for structural materials; owing to the lowest density and well-preserved SiC struts, sample SiC-l with the best recoverability and thermal insulation performance could be employed as electromechanical strain sensors; whereas sample SiC-m with a moderate density, dense nanowire distribution, and competent mechanical stability could be favourable for applications as a catalyst support.

3.3 Organic solvent/oil absorption

Nanostructured materials with 3D porous structure, hydrophobicity, and good mechanical stability are promising candidates for organic solvents/oil absorption. To enable the applications as organic solvent/ oil absorbent, we transformed the wettability of SiCNW scaffold from hydrophilicity to hydrophobicity by using n-Octadecyltrichlorosilane (OTS) as surface modifier. The surface-modified SiCNW scaffolds exhibit a selective adsorption of low-viscosity organic solvents. It is demonstrated that a piece of surface modified SiCNW scaffold was highly hydrophobic with a water contact of ~137.6° and can support a water droplet on its surface, while the oil droplet (coloured by methylene blue) was completely absorbed (Fig. S6). The ultrafast absorption with high capacity is examined. As shown in Fig. 5(a), 0.5 g toluene (dyed with Sudan III) on the water was completely absorbed by a piece of SiCNW scaffold within 2s. Furthermore, a droplet of chloroform (coloured with Sudan III) can be also rapidly absorbed (Fig. 5(b)).

The recoverability of contaminants and durability of sorbents are essential for the clean-up of chemicals, since these pollutants are either precious or poisonous. Direct combustion and mechanical squeezing have emerged to be the common approaches, in this study, SiC-m and SiC-l were chosen to demonstrate the two methods, respectively. As shown in Fig. 5(c), benefiting from the mechanical and thermal stability and fire-retardance, ethanol absorbed by the SiC-m sample can be removed by burning off, unlike carbon materials that experience apparent shrinkage and weight loss during burning process [17,18], the architecture and weight of the original scaffold remains unchanged. By contrast, the precious or toxic contents can be removed and recollected by mechanically squeezing the scaffold. Toluene was recollected by squeezing the elastic SiC-l scaffold (Fig. 5(d)), in the first cycle, 1126 mg of Toluene was absorbed, but the remnant mass was up to 645 mg after squeezing due to incomplete compression of the scaffold, however, the remnant weight remained unchanged from the second cycle. The SiCNW scaffolds retain the high adsorption capacity during 10 cycles of combustion or squeezing (Fig. 5(e) and (f)), the results clearly show the good recyclability of the SiCNW scaffold as an absorbent.

Based on the above results, the absorption capacities (Q (wt.%), defined as the ratio of as-obtained weight of SiCNW scaffold after full absorption to the initial weight) of SiCNWs scaffolds to various organic solvents and oils were further studied, possessing 15-38 times of their initial weight for the absorption of organic solvents or oils dependent on the density of liquid (Fig. 5(g)). This capability is much higher than previously reported melamine foam-templated SiC foams (1.1-4 times) [19], comparable to superhydrophobic microporous polymers (6-33 times) [20], wool-based nonwoven material (10-28 times) [21], and SiO_2 micro/nanofibrous membranes (34-43.7 times) [22].

The absorption mechanism of the SiCNW scaffolds is considered the physical absorption of organic molecules. Benefitting from the high porosity and unique complex dual structures, SiCNW scaffolds possessed an ultrafast absorption rate with ultrahigh capacity for organic solvents and oils, suggesting their potential applications for the facile removal of chemical spills and oil leakage and the ease of recycling.

3.4 Catalyst support for MB decomposition

Catalyst support is considered as one of the most primary functions of porous ceramic, especially for nanowire structures possessing large specific surface areas. In this context, we designed experiments to verify this by examining the capability of loading metal-organic framework (MOF)-derived photocatalyst, which we believe is of greater interests than loading traditional catalyst

particles. Meanwhile, we hope to tackle the two existing issues of porous ceramic-supported catalyst: (1) The agglomeration of metal oxides due to the high surface energies [23]; (2) The weak interaction between SiC and noble metal nanoparticles [24], which resulted in low activity and poor durability. In this regard, sample SiC-m with large amounts of SiCNWs, good interconnectivity, competent mechanical strength and high stability was chosen as the support for the in-situ synthesis of MOF-derived TiO_2-C. Auxiliary experiments using the traditional method of dip-coating the SiC scaffold with catalyst were also conducted to prepare specimens, as a reference. After a series of treatment of solvothermal reaction, centrifugation, washing, drying, and carbonisation, we have uploaded 17.5 mg MOF-derived Ti_2O-C catalyst on a 250 mg SiC-m scaffold, which was ~ 35 wt.% more than the dip-coating method (13 mg TiO_2-C catalyst uploaded). As displayed in the XRD patterns in Fig. 6(a), crystallised rutile and anatase polymorph TiO_2 particles were successfully identified, without noticeable changes to the SiC phase. Further examination confirmed that this in-situ synthesis resulted in TiO_2/C particles firmly attached to and uniformly embedded in the SiCNW scaffold (inset of Fig. 6(a)).

Fig. 6(b) displays the photocatalytic performance of samples for the photodegradation of MB solution under UV-visible light irradiation. The pure SiCNW scaffold demonstrated a certain degree of adsorption capacity, with 35.5% of MB being adsorbed and stored in the nanowire-constructed pores [25], and photodegraded due to the inherent photocatalytic capability of SiCNWs [26]. For the in-situ grown TiO_2-C/SiC samples, the MB was fully decomposed after 3 h of photocatalytic reaction (Fig. S7), much more effective than that of the dip-coated TiO_2-C/SiC, which was owing to the good access of light into the structure and higher catalyst loading for the in-situ samples. The plots of $\ln(C/C_0)$ *vs* irradiation time showed that the photodegradation reaction followed the first-order kinetics (Fig. 6(c)). After three cycles of photodegradation testing, there was negligible change (Fig. 6(d)), which demonstrates the good repeatability for the in-situ grown composite samples. These results have shown that the samples could be further developed for practical photocatalytic applications.

3.5 Electromechanical strain sensor

Owing to the relatively good recoverability under cyclic compressive load, the SiC-l scaffold was envisaged as electromechanical strain sensor, and its strain-dependant electrical response of SiCNW-l scaffold under cyclic compressive loading-unloading process was investigated. Fig. 7(a) and (b) show the intercepted variation of normalised electrical resistance (R_t/R_0) within cycles of 1-10 and 90-100. The value of R_t/R_0 decreased by ~24% in the first cycle under a 20% compressive

strain. Meanwhile, the values under both loading and unloading conditions kept dropping in the 2-5 cycles and fluctuating in 6-10 the cycles. However, the variation of the value gradually stabilised, as it switched in the range of 65-75% within the cycles 90-100. When the ε was increased to 30%, the value of R_t/R_0 decreased dramatically by ~60% in the first cycle, but more quickly stabilised from the 5^{th} cycle. This can be ascribed to the more complete plastic deformation of the scaffold subjected to the compression with the larger strains, which gives rise to unrecoverable deformation of the structure. Eventually, the value of R_t/R_0 switched stably in the range of 42-70%, larger than that under ε=20%.

The rational of the SiCNW scaffold sensor can be proposed from the mechanical deformation of the scaffold. When an external force is applied to sample SiCNW-l, the dual-structures are brought into a slight contact, leading to the formation of a temporary network for electrons to pass through. As a result, the electrical resistance reduced. Once the force is withdrawn, the resistance recovers [27]. In the first several cycles, the unrecoverable plastic deformation increases gradually with the increase in cycle, an accumulation of new conductive network is achieved, causing the drifting of the R_t/R_0 to lower values [28]. With the progress of cyclic loading-unloading process, some SiCNW and struts experience deformation and failure, leading to the interrupted conduction and slightly increased resistance output. Eventually, the new conductive network was formed via the stabilisation of cyclic compression, and the value of R_t/R_0 was quite constant, demonstrating good piezoresistive recoverability and reproducibility of the scaffolds.

4. Conclusion

In summary, we have successfully developed lightweight, multifunctional 3D SiCNW scaffolds using a catalyst-free, controllable replica-template method. The microstructural characteristics and properties of the scaffolds can be easily tuned by controlling the composition and solid loading (via compression) of the preceramic slurries. Benefiting from the unique open porous structure and the co-existence of SiC nanowires and struts, the resulting SiCNW scaffolds demonstrate strong yet flexible features with cyclic compressive responses, great thermal insulation and fire-retardance performance.

These excellent and tuneable properties make the SiCNW scaffolds a promising candidate as an efficient absorbent for organic solvents and oils, as catalyst supports with enhanced photocatalytic performance, and as competent electromechanical strain sensors for crucial environments. Owing to the suitability for large-scale production and versatility of achieving arbitrary shapes, it is envisaged

that these SiCNW scaffolds may find niche applications in filtration, thermal insulation, and a series of energy storage.

Declaration of Competing Interest

The authors report no declarations of interest.

Acknowledgements

The present work was supported by the National Natural Science Foundation of China (Grant No 51972068) and Key Laboratory of New Processing Technology for Nonferrous Metals and Materials (Guangxi University).

References

[1] J.H. Jing, H.Y. Wu, Y.W. Shao, X.D. Qi, J.H. Yang, Y. Wang, ACS Appl. Mater. Interfaces 11 (2019) 19252–19259.

[2] X. Liang, Y. Li, J. Liu, S. Sang, Y. Chen, B. Li, C.G. Aneziris, Ceram. Int. 42 (2016) 13091–13097.

[3] P. Colombo, H.P. Degischer, Adv. Eng. Mater. 14 (2012) 1051.

[4] J. Lee, D. Choi, C. Kim, S. Lee, S. Choi, Processing 8 (2007) 87–90.

[5] B. Li, X. Yuan, Y. Gao, Y. Wang, J. Liao, Z. Rao, B. Mao, H. Huang, Mater. Res. Express 6 (2019) 045030.

[6] M. Zhang, J. Zhao, Z. Li, H. Yu, Y. Wang, A. Meng, Q. Li, J. Solid State Chem. 243 (2016) 247–252.

[7] S. Li, H. Li, Q. Su, X. Liu, H. Zhao, M. Ding, K. Liu, W. Nie, Mater. Lett. 199 (2017) 113–115.

[8] J. Zhu, J. Jia, F.L. Kwong, D.H.L. Ng, Diam. Relat. Mater. 33 (2013) 5–11.

[9] H. Guo, P. Warnicke, M. Griffa, U. Müller, Z. Chen, R. Schaeublin, Z. Zhang, M. Luković, ACS Nano 13 (2019) 14337-14347.

[10] X. Zheng, H. Lee, T.H. Weisgraber, M. Shusteff, J. DeOtte, E.B. Duoss, J.D. Kuntz, M.M. Biener, Q. Ge, J.A. Jackson, S.O. Kucheyev, N.X. Fang, C.M. Spadaccini, Science 344 (2014) 1373–1377.

[11] C. Ferraro, E. Garcia-Tuñon, V.G. Rocha, S. Barg, M.D. Fariñas, T.E.G. Alvarez-Arenas, G. Sernicola, F. Giuliani, E. Saiz, Adv. Funct. Mater. 26 (2016) 1636–1645.

[12] L. Su, M. Li, H. Wang, M. Niu, D. Lu, Z. Cai, ACS Appl. Mater. Interfaces 11 (2019) 15795–15803.

[13] M.A. Worsley, S.O. Kucheyev, J.H. Satcher, A. V. Hamza, T.F. Baumann, Appl. Phys. Lett. 94 (2009) 1–4.

[14] F. Wang, L. Dou, J. Dai, Y. Li, L. Huang, Y. Si, J. Yu, B. Ding, Angew. Chemie 59 (2020) 8285–8292.

[15] S. Vijayan, P. Wilson, R. Sreeja, K. Prabhakaran, Mater. Lett. 194 (2017) 126–129.

[16] S. Chabi, V.G. Rocha, E. Garclá-TunÌón, C. Ferraro, E. Saiz, Y. Xia, Y. Zhu, ACS Nano 10

(2016) 1871–1876.

[17] Z. Wu, C. Li, H. Liang, J. Chen, S. Yu, Angew. Chemie - Int. Ed. 125 (2013) 2997–3001.

[18] Y. Hu, Z. Chen, H. Zhuo, L. Zhong, X. Peng, R. Sun, Adv. Funct. Mater. 29 (2019) 1904472.

[19] L. Luo, X. Chen, Y. Wang, J. Yue, Z. Du, X. Huang, X.Z. Tang, Ceram. Int. 44 (2018) 12021–12029.

[20] A. Li, H.X. Sun, D.Z. Tan, W.J. Fan, S.H. Wen, X.J. Qing, G.X. Li, S.Y. Li, W.Q. Deng, Energy Environ. Sci. 4 (2011) 2062–2065.

[21] M.M. Radetić, D.M. Jocić, P.M. Jovančić, Z.L. Petrović, H.F. Thomas, Environ. Sci. Technol. 37 (2003) 1008–1012.

[22] Z. Liu, Y. Tang, K. Zhao, Q. Zhang, Colloids Surfaces A Physicochem. Eng. Asp. 568 (2019) 356–361.

[23] M.Z. Hussain, G.S. Pawar, Z. Huang, A.A. Tahir, R.A. Fischer, Y. Zhu, Y. Xia, Carbon N. Y. 146 (2019) 348–363.

[24] C. Han, Y. Wang, Y. Lei, B. Wang, Ceram. Int. 42 (2016) 5368–5374.

[25] L. Su, H. Wang, M. Niu, X. Fan, M. Ma, Z. Shi, S.-W. Guo, ACS Nano 12 (2018) 3103-3111.

[26] R. Wu, K. Zhou, C.Y. Yue, J. Wei, Y. Pan, Prog. Mater. Sci. 72 (2015) 1–60.

[27] L. Zhao, F. Qiang, S.-W. Dai, S.-C. Shen, Y.-Z. Huang, N.-J. Huang, G.-D. Zhang, L.-Z. Guan, J.-F. Gao, Y.-H. Song, L.-C. Tang, Nanoscale 11 (2019) 10229-10238.

[28] H. Liu, W. Huang, J. Gao, K. Dai, G. Zheng, C. Liu, C. Shen, X. Yan, J. Guo, Z. Guo, Appl. Phys. Lett. 108 (2016) 011904.

Figure Captions

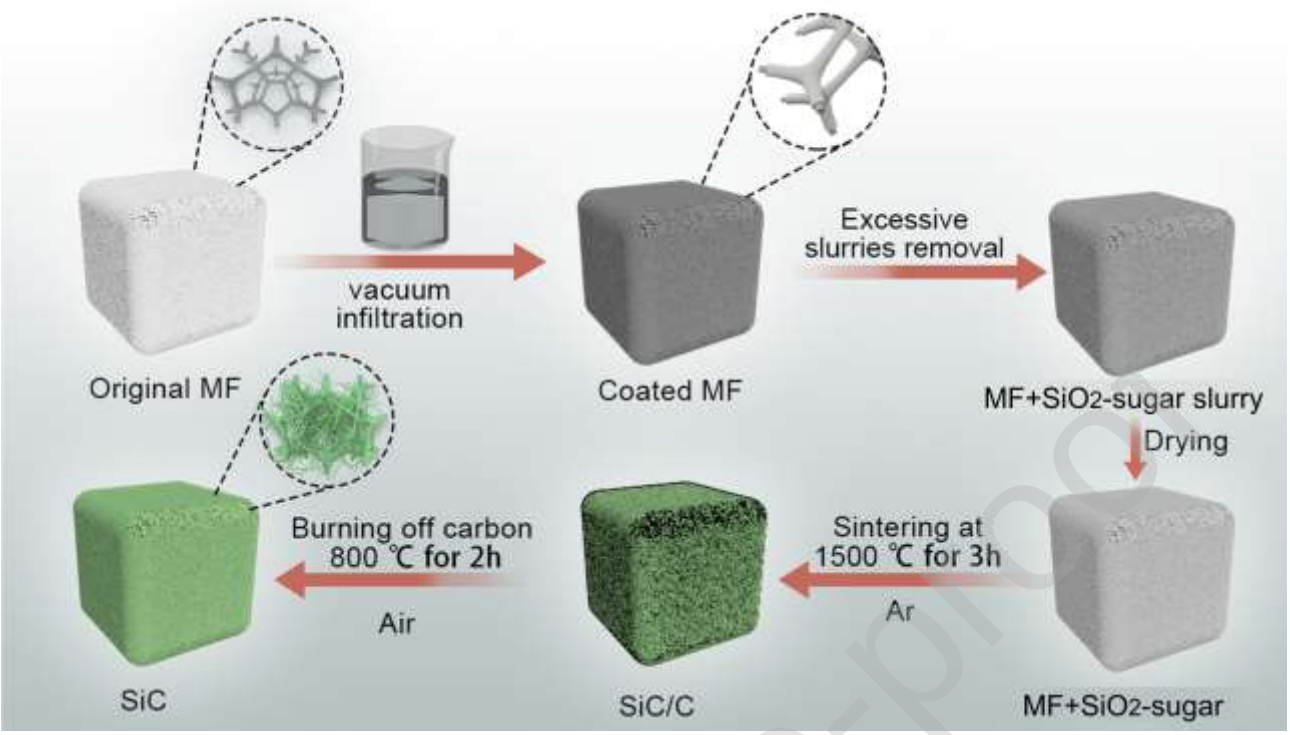

Fig. 1. Schematic of the fabrication processes of the melamine foam-templated growth of SiC scaffolds.

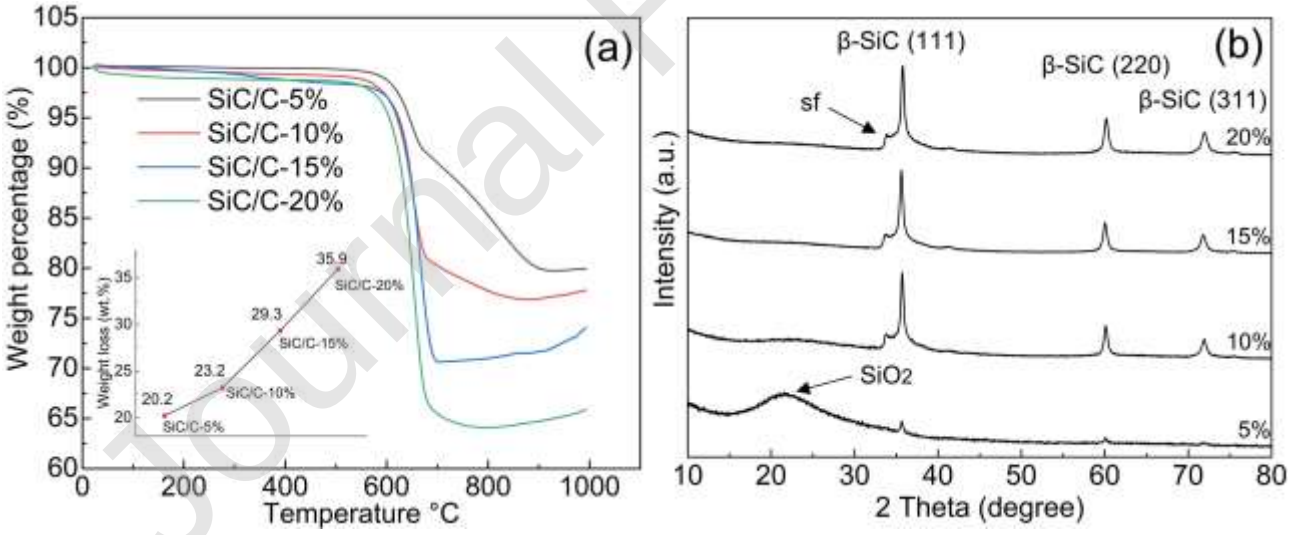

Fig. 2. (a) TGA result and (b) XRD patterns of the as-obtained SiC/C before the carbon removal treatment. Inset in (a) showing the weight loss of all the samples.

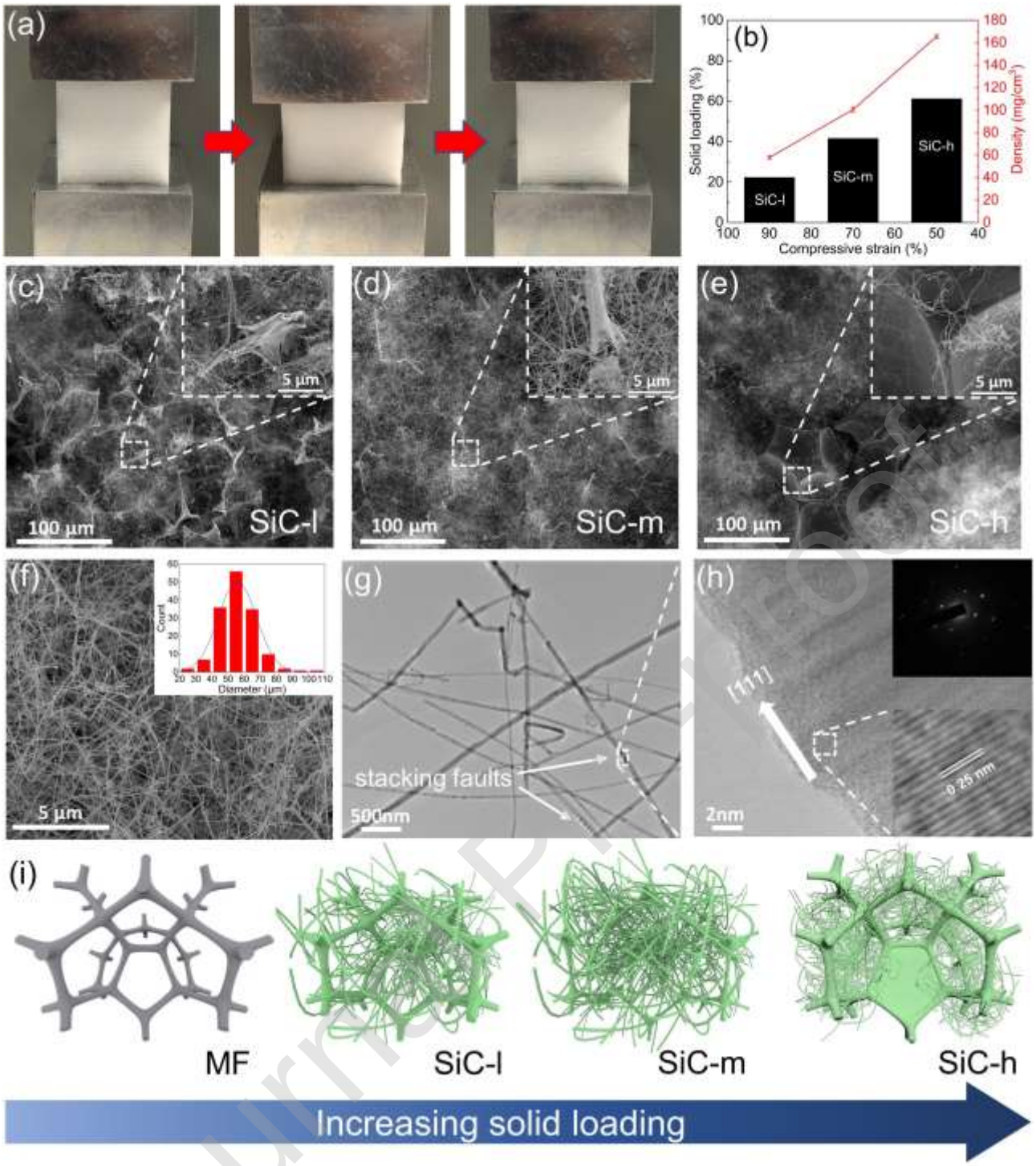

Fig. 3. (a) Schematic of the impregnated MF subjected to compressions for quantitively removing the excessive slurries. (b) The relationship of applied compression strain *vs.* solid loading on the MF and the final density of the SiC scaffolds. SEM images of (c) SiC-l, (d) SiC-m, and (e) SiC-h, respectively. (f) High magnification SEM image of SiCNWs, and the inset showing the diameter distribution profile. (g) TEM image of the SiCNWs. (h) High-resolution TEM image of a SiCNW. The top-right inset is the SAED pattern of the nanowire. The bottom-right inset is a partially enlarged drawing showing the spacing between two adjacent lattice planes. (i) Drawing illustrating the effect of solid loading on the microstructures of resultant SiCNW scaffolds.

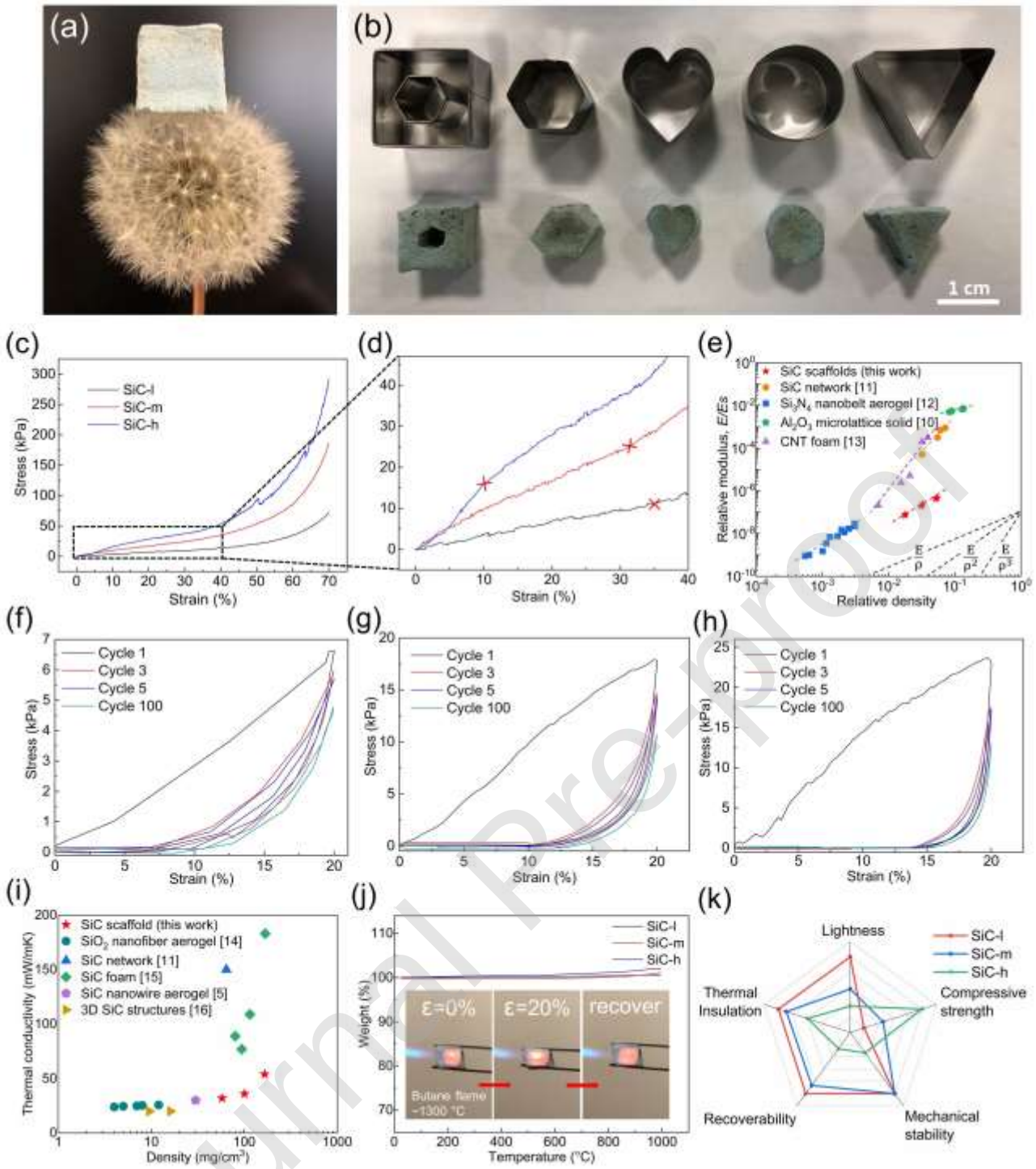

Fig. 4. (a) Light-weight SiC-l scaffold supported by a dandelion. (b) The resultant SiCNW scaffolds with different shapes that originated from different moulds. (c, d) Compressive stress-strain curves of the SiC-l, SiC-m, and SiC-h scaffolds, the crosses in (d) indicate the end of elastic region. (e) Dependence of the relative modulus on the relative density for the SiCNW scaffolds and other reported materials. (f-h) Cyclic compressive stress-strain curves of samples SiC-l, SiC-m, and SiC-h at a ε = 20%, respectively. (i) The thermal conductivity of the as-obtained SiCNW scaffolds against other reported porous SiC structures. (j) TGA profile of the thermal stability for the present SiCNW scaffold. Inset shows a digital photo of the compression and recovery process of SiC-l in the flame

of a butane blowtorch. (k) A spider chart comparing the porosity, compressive modulus, mechanical stability, recoverability, thermal insulation effects of different samples.

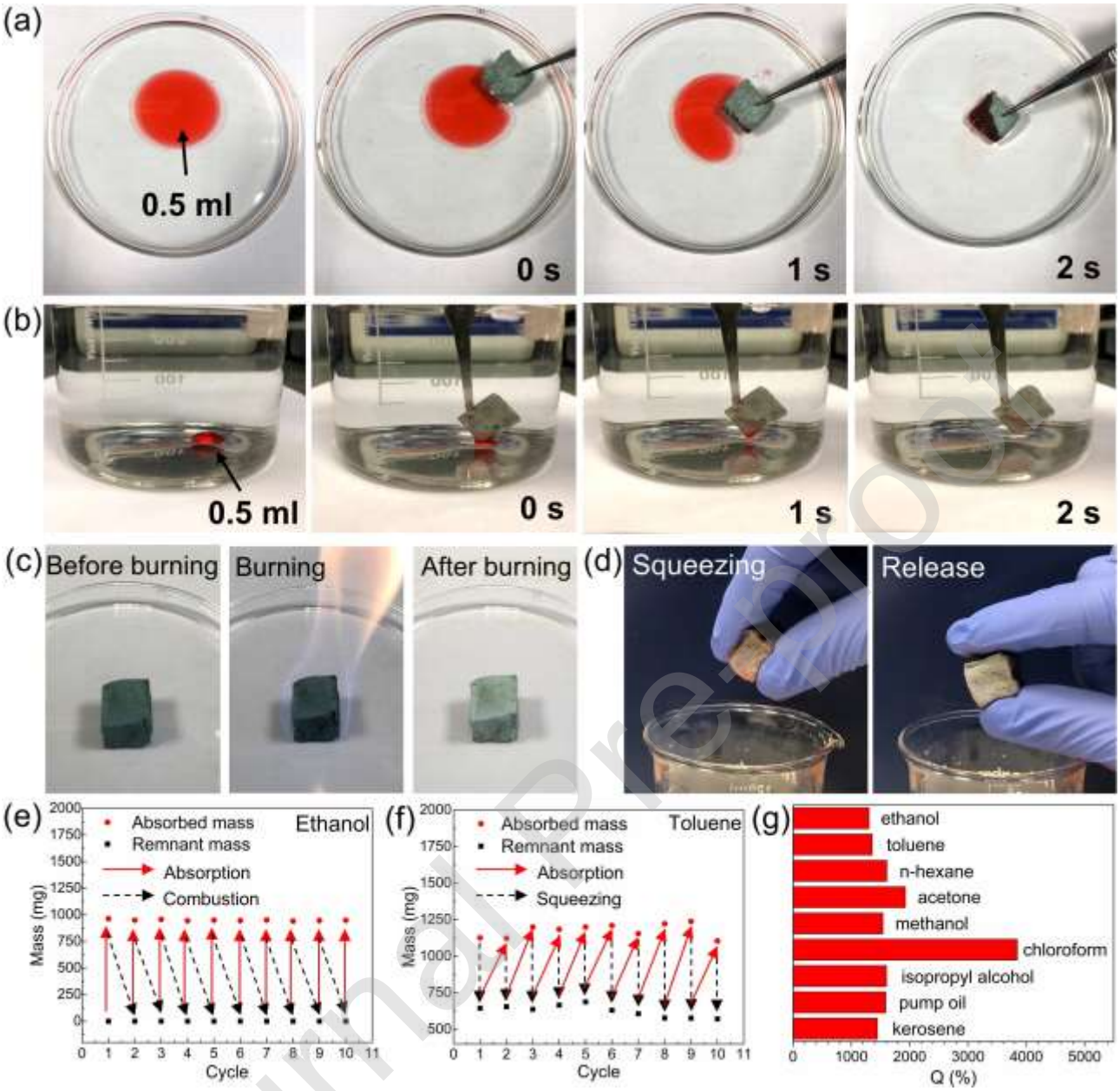

Fig. 5. Oil and organic solvent absorption properties of the SiCNW scaffold. (a) Digital photos demonstrating the absorption process of toluene (coloured with Sudan III for clear presentation) within 2 s. (b) Digital photos demonstrating the absorption process of chloroform (coloured with Sudan III for clear presentation) within 2 s. (c) Recycling process of SiC-m by combustion. (d) Recycling process of SiC-l by squeezing. (e) Recyclability of the SiCNW scaffold for absorption of ethanol when using combustion method. (f) Recyclability of the SiCNW scaffold for absorption of Toluene when using squeezing method. (g) Absorption capability of the SiCNW scaffold for various organic liquid and oils.

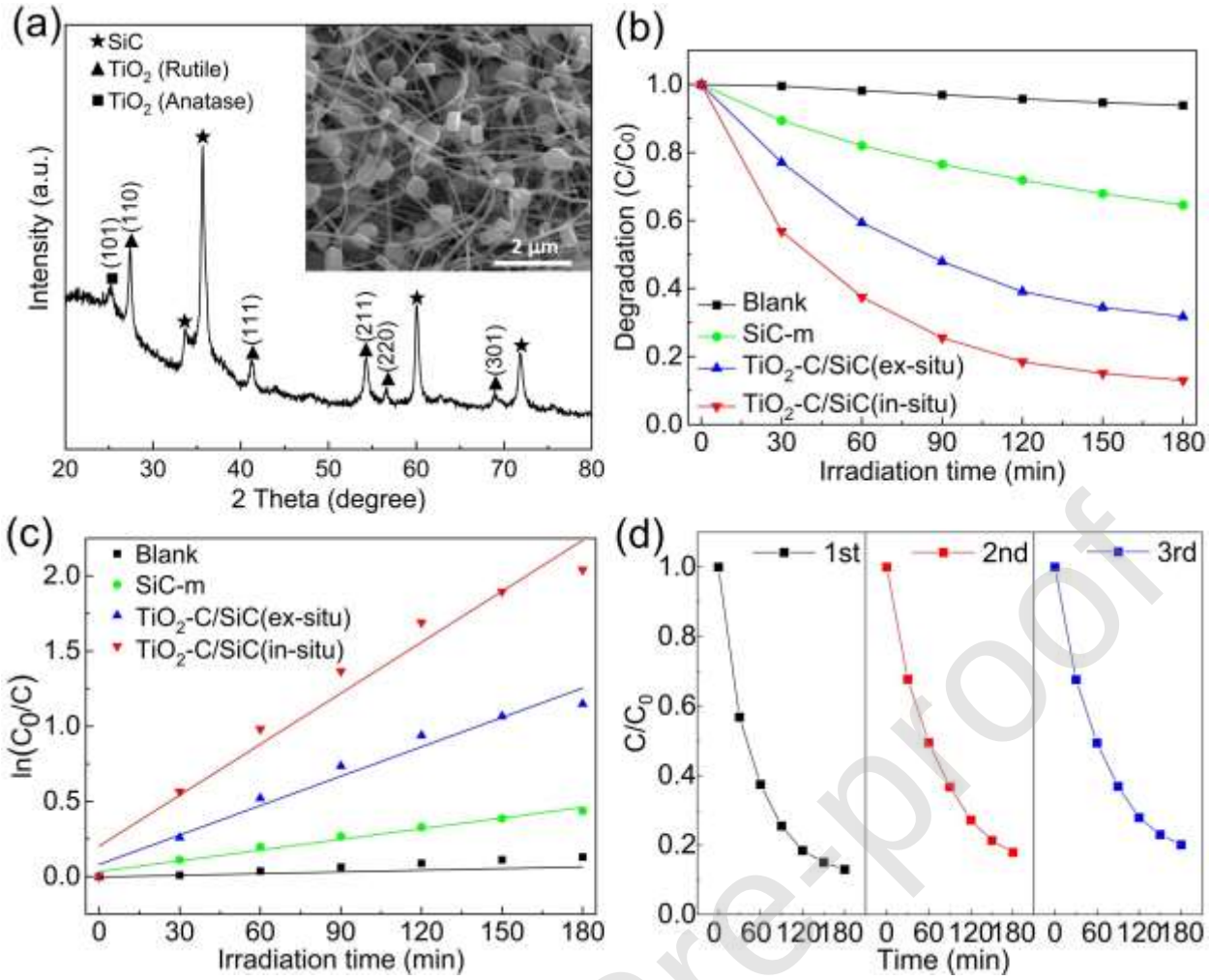

Fig. 6. (a) XRD profile of the TiO_2-C/SiC composites, inset showing the SEM image. (b) Photodegradation of MB and (c) kinetic curves for photodegradation of MB by pure SiC, TiO_2-C/SiC (*in-situ*), TiO_2-C/SiC(*ex-situ*) under UV-visible light irradiation. (d) Recyclability test of TiO_2-C/SiC(*in-situ*) composites for photodegradation of MB under UV-visible light irradiation.

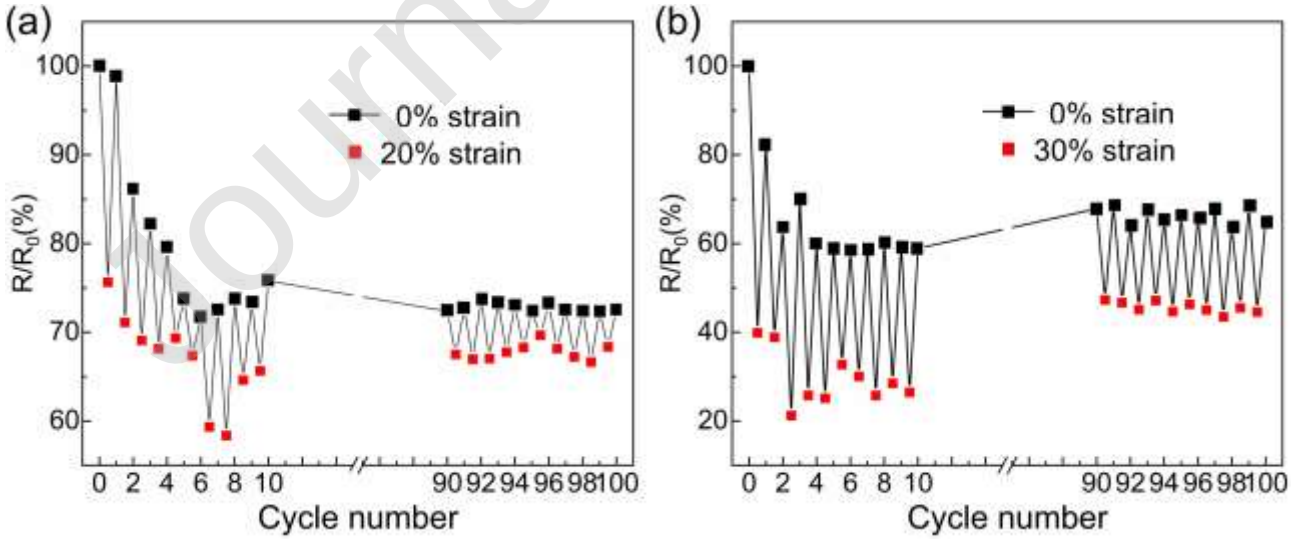

Fig. 7. Normalised electrical resistance changes of SiC scaffolds under 100 cyclic compressive loading-unloading tests at ε of 20% and 30%, respectively.